Nonlinear Model Predictive Control for Thermal Management in Plug-in Hybrid Electric Vehicles

J. Lopez-Sanz, Carlos Ocampo-Martinez *Senior Member, IEEE*, Jesus Alvarez-Florez, Manuel Moreno-Eguilaz, Rafael Ruiz-Mansilla, Julian Kalmus, Manuel Gräeber, Gerhard Lux

***Abstract*—A nonlinear model predictive control (NMPC) for the thermal management (TM) of Plug-in Hybrid Electric Vehicles (PHEVs) is presented. TM in PHEVs is crucial to ensure good components performance and durability in all possible climate scenarios. A drawback of accurate TM solutions is the higher electrical consumption due to the increasing number of low voltage (LV) actuators used in the cooling circuits. Hence, more complex control strategies are needed for minimizing components thermal stress and at the same time electrical consumption. In this context, NMPC arises as a powerful method for achieving multiple objectives in Multiple input- Multiple output systems.**

This paper proposes an NMPC for the TM of the High Voltage (HV) battery and the power electronics (PE) cooling circuit in a PHEV. It distinguishes itself from the previously NMPC reported methods in the automotive sector by the complexity of its controlled plant which is highly nonlinear and controlled by numerous variables. The implemented model of the plant, which is based on experimental data and multi- domain physical equations, has been validated using six different driving cycles logged in a real vehicle, obtaining a maximum error, in comparison with the real temperatures, of 2°C.

For one of the six cycles, an NMPC software-in-the loop (SIL) is presented, where the models inside the controller and for the controlled plant are the same. This simulation is compared to the finite-state machine-based strategy performed in the real vehicle. The results show that NMPC keeps the battery at healthier temperatures and in addition reduces the cooling electrical consumption by more than 5%. In terms of the objective function, an accumulated and weighted sum of the two goals, this improvement amounts 30%. Finally, the online SIL presented in this paper, suggests that the used optimizer is fast enough for a future implementation in the vehicle.

***Index Terms*—nonlinear model predictive control (NMPC), thermal management, plug-in hybrid electric vehicles (PHEV), Li-ion battery cooling.**

The authors wish to acknowledge financial support from the Generalitat de Catalunya (GRC MCIA, Grant n SGR 2014-101).

J. Lopez-Sanz and G. Lux are with Innovation and Alternative Mobility Department, SEAT Technical Center, Autovia A-2, Km. 585 Apdo. de Correos 91, 08760 Martorell, Spain, e-mails: jorge.lopez1@seat.es, gerhard.lux@seat.es

C. Ocampo-Martinez is with Automatic Control Department, Universitat Politècnica de Catalunya, Institut de Robòtica i Informàtica Industrial (CSIC-UPC), Llorens i Artigas, 4-6, 08028 Barcelona, Spain, e-mail: cocampo@iri.upc.edu

J. Alvarez-Florez is with the Center for Engines and Heat Installation Research (CREMIT), Technical University of Catalonia, Barcelona Tech., 08028 Barcelona, Spain, e-mail: jalvarez@mmt.upc.edu

M. Moreno-Eguilaz is with the Center Innovation Electronics, Motion Control and Industrial Applications (MCIA), Technical University of Catalonia, Barcelona Tech., 08028 Barcelona, Spain, e-mail: manuel.moreno.eguilaz@upc.edu

R. Ruiz-Mansilla is with the Green Technologies Research Group (GREENTECH), Technical University of Catalonia, Barcelona Tech.,08028 Barcelona, Spain, e-mail: rafael.ruiz@upc.edu

J. Kalmus works at TLK-Thermo GmbH, Hans-Sommer-Str.5, 38106 Braunschweig, Germany, e-mail: j.kalmus@tlk-thermo.de

M. Gräber works at TLK Energy GmbH, Steppenbergweg 30, 52074 Aachen, Germany, e-mail: manuel.graeber@tlk-energy.de

This work was supported by the catalan Government: la Generalitat de Catalunya. Corresponding author: Jorge Lopez-Sanz extern.jorge.lopez@seat.es

I. Introduction

Electromobility is a necessary step for car manufacturers to fulfill the increasing stringent emissions legislation. Although some pure electric vehicles (EV) are already available in the market, Plug-in Hybrid Electric Vehicles (PHEVs) seem to be the middle-term solution till infrastructure and costumers' demand grows [1].

Electrification involves several technical challenges. Among them, the Thermal Management (TM) of the electric components is crucial for assuring safety, performance and durability requirements [2]. In this context, the high voltage (HV) battery pack is of first interest due to its high cost. Li-ion batteries, which are the state of the art and future technology in electromobility [3], [4], have to operate within a certain temperature range for safety, optimum performance and service life. The range recommended by the battery manufacturer (typically 20°C-30°C) is usually narrower than the vehicle operation range, which has to assure extreme hot (≈ 60°C) and cold (≈ -25°C) climates. To fix this temperature offset,

several TM approaches exist in literature which can be divided according to the heat transfer medium used: air [5], [6], liquid or phase change material (PCM) [7], [2], [8]. The choice of the transfer medium depends on the vehicle topology and is finally a trade-off between performance, durability and costs.

In the case of PHEVs, using only PCM may not be applicable [9] and most automakers face the decision of either using air or liquid cooling. While air systems are, in general, simpler and more economic, liquid solutions offer more effectiveness in heat transfer and more accuracy in the temperature control [10]. However, a better temperature regulation is at the prize of higher costs and a more complex design and control. Given a complex design of intricate pipes architecture, the challenge in the liquid TM control strategy is to use the numerous electrical actuators such as pumps, valves and fans to keep the battery within the optimal operation range consuming as less electrical energy as possible. This task can be especially complex, since liquid TM systems have usually:

- multiple inputs and multiple outputs
- high nonlinear behavior
- to fulfill multiple and often contradictory goals

At present, these complex battery TM systems are commonly controlled with finite-state-machines and PID controllers which use a set of rules learned from experience [11], [12]. However despite these methods are valid for vehicle operation within the current specifications, they are normally oversized and far away from optimum, particularly in the case of hybrid and electric vehicles where few experience is available.

Motivated by all the above, the aim of this paper is to propose a new control method to make liquid TM of the HV battery more attractive reducing its costs and complexity. The method presented here, Model Predictive Control (MPC), belongs to the family of methods based on optimal control and is especially suitable for finding solutions closed to the optimum in complex multi-objective controlled plants.

The main idea behind MPC is to combine a model of the controlled plant with an optimization algorithm. The model is used to predict the future state of the plant within a time horizon and the optimization algorithm to find the best possible control set inside this prediction horizon. Additionally to the model and the algorithm, an objective function for the numerical evaluation of the multiple goals to be optimized has to be provided. If the model used to describe the behavior of the controlled plant and/or the objective function are described by means of nonlinear functions, as is the case of this work, the method can be sub-categorized as Nonlinear Model Predictive Control (NMPC). Through the combination of the model and the optimization algorithm, MPC provides not only the best possible controls, but the following advantages compared to the conventional control methods:

- **Constraints direct specification:** in addition to the objective function, constraints which will fulfilled in the final solution can be specified quite straightforward.
- **No curse of dimensionality:** the complexity in the multiple feedback controllers design is similar as of single variable ones [13].
- **Future information exploitation:** given future information of the vehicle, e.g the driving profile that will be performed, the model can be painless modified to improve the quality of the predictions and hence of the final solution.

Due to the several advantages mentioned, considerable interest in this method has been shown in the automotive sector leading to MPC applications in several fields such as Internal Combustion Engines (ICEs) [14], [15], [16], autonomous vehicles [17], stability [18], idle speed [19] and energy management [20] among others.

In the TM branch most MPC efforts have been put in the cabin comfort [21] and the ICE cooling [22], in order to reduce consumption and emissions. Nevertheless, despite the HV battery is the core of the electrified vehicles, less attention has been put in MPC methods to improve its TM. To fill this gap we propose an NMPC control method which reduces the complexity and costs associated to the liquid TM in the HV battery (BAT) and power electronics (PE) cooling circuit in a real PHEV prototype. The method is used to improve the TM of the mentioned system with two different goals: 1) minimize the thermal stress of the BAT and 2) minimize the electrical consumption of the actuators in the cooling circuitl.

To perform these tasks, the robust optimization software package MUSCODII [23] is used and combined with a suitable modeling strategy and appropriate objectives and constraints specifications it achieves online performance. Experimental results with a hybrid Golf GTE are presented, demonstrating the validity of the proposed methodology. The validation is based on the comparison of the NMPC with the current implemented finite-state machine TM in the vehicle. The aim is to proof that high nonlinear systems with several goals and constrains find

in NMPC a more powerful control method in contrast to classical approaches.

This paper is structured as follows. Sections II and III present the controlled plant and the corresponding developed model; the next sections (IV, V and VI) deal with the mathematical and control backgrounds of the NMPC technique; afterwards, the used vehicle data acquisition system is described in VIII and the model is validated with the help of measurements logged in several real driving cycles. Finally, in section IX, the potential of the optimizer will be addressed by means of an online optimization followed by conclusive remarks.

II. Description of the Thermal System

PHEVs can be powered by an internal combustion engine (ICE), by an electric machine (EM) or by a combination of both. Conventional traction components (ICE, clutch, gearbox) have different temperature operating ranges compared to the high sensible electrical ones: EM, power electronics (PE), HV battery and charger. This leads to complicated designs as in the case of the studied PHEV [24], which contains three separated cooling circuits:

- A high temperature circuit (HT) for the ICE, gearbox and cabin heaters with operating points above 90°C.
- A low temperature circuit (LT1) for the EM, turbocharger and the charge air cooler with maximal operating temperatures between 75 and 90°C.
- A second low temperature circuit (LT2) for the Li-Ion HV Battery, PE and Charger, with temperatures below 60°C.

In this research we study the LT2 circuit whose aim is to dissipate the generated heat in three sources: Charger, Battery and PE. Nevertheless notice that during driving, the charger is not a heat source, since no electric current flows through it.

In order to dissipate the generated heat, two heat sinks are present: the cooler and the chiller. The cooler is an U-form tubular heat exchanger located on the front of the vehicle (in front of three other heat exchangers: the HT-, LT1 coolers and the condenser). It allows the heat transfer to the air. The chiller is a heat exchanger that performs heat transfer to the vehicle Air Conditioning (AC) circuit.

The transfer medium is a water/glycol mixture and works depending on six electrical actuators, as shown in Fig. 1 in gray clockwise: cooler valve, Fan, BAT pump, chiller valve, circuit valve and PE pump.

The solenoid valves are electromechanically operated and have only two possible positions. The pumps and fan are regulated by means of a pulse width modulated

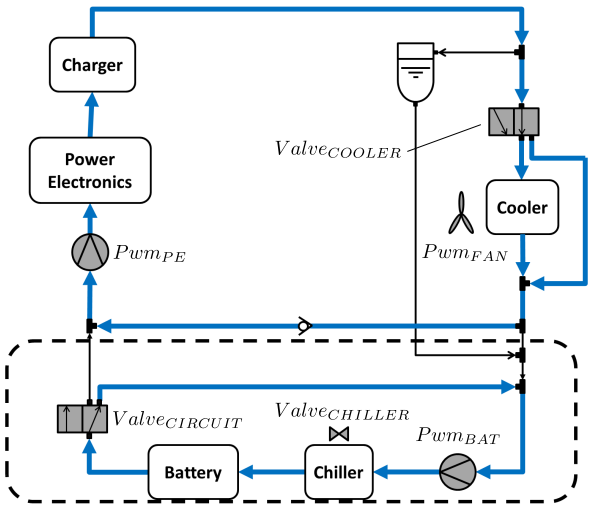

Fig. 1. LT2 Circuit with two possible operation modes.

(PWM) signal. The cooler valve is used to force the coolant flow through the cooler or bypass it. The Fan, which is shared by the three circuits, is used to assure enough air mass flow through the cooler when the vehicle speed is low. The chiller valve allows the coolant flow to transfer heat to the AC. Finally, the pumps and the circuit valve, as shown in Fig. 1, are responsible for two possible configurations:

- Two-circuit mode: The circuit valve disables the flow through the black tube outlet and enables the flow through the blue one, thus separating both circuits. The resulting independent battery circuit can be seen in the dotted rectangle in Fig. 1.
- One-circuit mode: The circuit valve disables the flow through the blue tube outlet in Fig. 1 and enables it through the black one, connecting this way the PE and Battery circuits.

The pumps guarantee that the coolant flows as needed in every circuit configuration. It is important to remark that in both modes, the coolant can flow through the blue horizontal tube above the battery circuit. This can only be done in one direction, thanks to a non-return valve as shown in Fig. 1. Finally, a compensation tank works as hydraulic protection.

The basic idea behind the LT2 design is to ensure that the Li-Ion battery operates at healthy temperatures. In the one-circuit-mode, the BAT can be warmed up or cooled down, while in the two-circuits-mode, it can be only drastically cooled down by means of the chiller. This last mode is only desirable at extreme cases, since the heat dissipation to the AC implies an overload to the HV electrical compressor in the refrigeration cycle. In the two-circuits-mode it is also possible to balance the

battery cells.

III. The Model for Thermal Management

Modelling is the real bottleneck for NMPC to become a standard control design method for the automotive industry [25]. Suitable models should describe the real dynamics accurately while being fast enough for computation. To obtain an accurate and efficient system model, a combination of physical and data-based methods was developed using the commercial environment Dymola [26]. This is a software tool based on the object-oriented language Modelica. The model consists of a set of explicit ordinary differential equations (ODEs) describing the dynamic behaviour of the LT2 circuit in terms of thermodynamic, electrical and flow balances. This multi-disciplinary approach can be seen in Fig. 2, where the hydraulic, thermal, LV, HV and mechanical paths of the developed model are represented in different colors. The red dotted line in the chiller and the BAT represents the connection of these two components, that for clarity was not done with a solid line. The same applies to the currents of the actuators where the orange dotted lines would end all in the drain $I_{Actuators}$.

A key aspect when modelling for NMPC is to avoid discontinuities from where the optimization algorithm cannot continue. To solve this, the object-oriented component model library TIL was used. TIL was developed within the scope of the thesis [27] and in its "Utilities" package, there are several smooth transition functions provided. For this research, the smooth transition with $n = 1$ was selected.

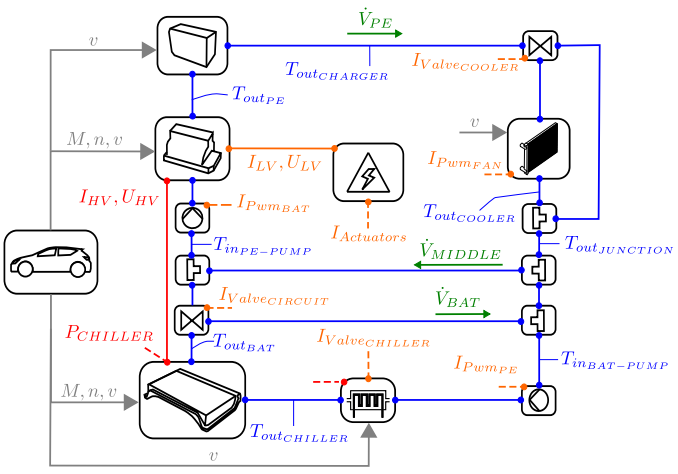

Fig. 2. Multi-domain model of the LT2 Circuit with mechanical (grey), LV (orange), HV (red), thermal (blue) and hydraulic representative variables (green).

In the next subsections, the model underlaying physics will be described according to the different domains.

A. Thermal domain

The thermal behavior of the components (PE, BAT and charger) is described by means of the first law of thermodynamics:

$$\frac{dU}{dt} = \dot{Q}_{thm} = \dot{Q}_{induced} - \dot{Q}_{ambient} - \dot{Q}_{coolant}, \quad (1)$$

where the heat flows are described by means of Eq. (2), being m, c, A, ϵ the component mass, specific heat capacity, surface and emissivity respectively, σ is the Boltzmann constant and α is the convection coefficient for the component-air heat transfer calculated with the empirical Nusselt correlations for forced air convection in flat plates [28]. The emissivity ϵ was taken constant 0.8 and finally the heat capacity $m \cdot c$ and A of the component were calibrated with experimental measurements. The fluid heat capacity c_p and other properties such as the density are calculated by means of TILMedia® (TLK Thermo GmbH), a library optimised for stable and quick dynamic simulations of this kind of systems [27]. The induced heat flow in the components is caused by ohmic heating and according to Eq. (1) is dissipated in the air, the coolant and the thermal mass of the components. The conduction losses were considered negligible compared to the other losses. The heat transfer to the coolant is done by means of cooling plates. The equations in the T junction pipes shown in Fig. 2 are also a thermal balance as Eq. (1),neglecting losses to the environment and with no heat induction.
Similarly to the heat sources, the heat sinks (cooler and chiller) balances are:

$$\dot{Q}_{thm} + \dot{Q}_{dissipated} + \dot{Q}_{ambient} + \dot{Q}_{coolant} = 0 \quad (3)$$

The dissipated heat flow through the cooler is determined with the Number of Transfer Units (NTU) Method:

$$\dot{Q}_{dissipated} = h(\dot{V}, \dot{m}_{air}) \cdot (T_{inlet} - T_{ambient}) \quad (4)$$

where the heat capacity rate (h) was observed experimentally and stored in a look-up table with the air mass and the coolant volume flow rate as inputs. The inlet temperature of the air was assumed to be the ambient and its mass flow was determined with a polynomial that depends on the Pwm_{FAN} signal and the vehicle speed:

$$\dot{m}_{air} = f(v, Pwm_{FAN}) \quad (5)$$

In the chiller, the dissipated heat to the AC system is the experimental constant value of $1.2kW$ when active and 0 when disabled.

$$\dot{Q}_{thm}(t) = m\, c_{component}\, \frac{dT_{component}(t)}{dt} \tag{2a}$$

$$\dot{Q}_{ambient}(t) = \alpha(t)\, A\, (T_{component}(t) - T_{ambient}(t) + A\, \epsilon\, \sigma\, (T^4_{component}(t) - T^4_{ambient}(t)) \tag{2b}$$

$$\dot{Q}_{coolant}(t) = \dot{m}(t)\, c_p(t)\, (T_{outlet}(t) - T_{inlet}(t)) \tag{2c}$$

Furthermore, it was assumed that the coolant is incompressible and that the surface in contact between the refrigeration pipes and the heat source in the component is enough large to ensure a fast equilibrium and thus $T_{outlet} = T_{component}$. With all this, the temperature in every point of the circuit (blue variables in Fig. 2) can be calculated.

B. Hydraulic domain

The aim of the hydraulic part of the model was to calculate the coolant flow through the different pipes of the circuit represented in green in Fig. 2. For a better accuracy/simplicity trade-off, no pressure states were modeled. Instead, look-up tables generated with a high-fidelity hydraulic model in GT-SUITE software (Gamma Technologies, Inc.) were used. The look-up tables are contained in the pumps and in the cooler valve models and depend on the coolant temperature and the controls:

$$\begin{aligned}\dot{V}(t) = f(&T(t), Valve_{COOLER}(t), Valve_{CHILLER}(t),\\ &Valve_{CIRCUIT}(t), PWM_{FAN}(t),\\ &PWM_{PE}(t), PWM_{BAT}(t)).\end{aligned} \tag{6}$$

The coolant volume flow rate read in the look-up tables is passed along the circuit through the T junctions represented in Fig. 2 using simple flux continuity equations.

C. Electric domain

The electric domain consists of the LV and HV grids as shown in Fig. 2 in orange and red, respectively. The goal of the HV model is to describe the electrical losses in the components that are transformed in heat, $Q_{induced}$, due to the Joule effect. The PE module consists of the Inverter and the DC/DC converter. The LV is assumed to be constant 14V and the HV is defined as the open-circuit voltage stored in look up tables:

$$U_{HV} = f(SOC, T) \tag{7}$$

Where T is the BAT temperature and SOC is the state of charge relating the actual energy with the maximum:

$$SOC = \frac{E_{BAT}}{E_{BAT_{MAX}}} \cdot 100 \tag{8}$$

The HV power is calculated as:

$$P_{HV} = U_{HV} \cdot I_{HV} \tag{9}$$

The HV power increases or decreases the BAT energy and the Joule's first law determines the heat flow generated in this process:

$$\frac{dE_{BAT}(t)}{dt} = P_{HV}(t) + P_{loss_{BAT}}(t), \tag{10a}$$

$$\dot{Q}_{induced_{BAT}}(t) = P_{loss_{BAT}}(t) = R_i(t)\, I^2_{HV}(t), \tag{10b}$$

$$R_i(t) = f(SOC(t), T(t)), \tag{10c}$$

Where R_i was measured in charging and discharging tests.
The HV power depends on different demands:

$$P_{HV} = P_{chiller} + P_{car} + P_{LV} + Ploss_{PE}, \tag{11a}$$

$$P_{chiller} = \frac{\dot{Q}_{dissipated}}{COP}, \tag{11b}$$

$$P_{car} = f(M, n), \tag{11c}$$

$$P_{LV} = U_{LV}\, I_{LV}. \tag{11d}$$

Equation (11b) stands for the extra power demand to the HV compressor of the AC circuit when the chiller enables a dissipation of $1.2kW$. A coefficient of performance (COP) of 3 was taken. Equation (11c) corresponds to the electrical energy needed for the vehicle traction and it depends on the torque and rotational speed of the electric machine. The LV electrical demand, Eq. (11d), depends on the current of the LT2 circuit actuators and the average of all other LV consumers in the vehicle given by $I_{auxiliary}$:

$$\begin{aligned}I_{LV}(t) = &I_{PWM_{BAT}}(t) + I_{PWM_{PE}}(t) +\\ &I_{PWM_{FAN}}(t) + I_{Valve_{CHILLER}}(t) +\\ &I_{Valve_{COOLER}}(t) + I_{Valve_{CIRCUIT}}(t) +\\ &I_{auxiliary}.\end{aligned} \tag{12}$$

Finally, the heat losses in the PE module are calculated with Eq. (13):

$$\begin{aligned}\dot{Q}_{induced_{PE}}(t) &= P_{loss_{PE}}(t)\\ &= P_{loss_{PE_{HV}}}(t) + P_{loss_{PE_{LV}}}(t),\end{aligned} \tag{13}$$

where the HV losses in the inverter are calculated with

TABLE I
SIMULATION TIME.

Cycle	Duration(s)	Simulation(s)	Factor(-)
EMPA B	2024	4,89	>400
EMPA Bschl	963	2,97	>300
EMPA BAB	1000	1,05	>900

Eq. (14a) and the LV losses in the DC/DC converter are calculated with Eq. (14b) using a constant efficiency of $\eta = 90\%$:

$$P_{loss_{PE_{HV}}} = f(M, n, U_{HV}) \tag{14a}$$

$$P_{loss_{PE_{LV}}} = \frac{P_{LV} \cdot (1-\eta)}{\eta} \tag{14b}$$

D. Mechanical domain

The mechanical part of the model is just an interface to the real vehicle: rotational speed (n)-, torque (M) of the electric machine and vehicle speed (v) are read from several CAN buses and used as inputs for the calculations shown in the thermal and electric domains.

The resulting model contains around 500 equations, 1300 variables, 6 controls and 9 differentiated state variables, being hundreds of times faster than real time. This can be seen in Table I, where the average time of 5 simulations in three different driving cycles taken from [29] is shown.

To transcript the hundreds of equations in the model to the optimization tool with no errors and in the shortest possible time, the automated methodology proposed in [30] is used.

All in all, it can be said that the developed model is suitable for a posterior control, since it is simple enough but still captures the essential dynamics.

IV. Optimal Control Problem

As explained before, the dynamic behavior of the thermal system is described as a set of ODEs:

$$\frac{d(x)}{dt} = f(x(t), u(t), p), \qquad t\epsilon\tau, \tag{15}$$

where $x(\cdot)\epsilon\mathbb{R}^{n_x}$ are the differential states, $u(\cdot)\epsilon\mathbb{R}^{n_u}$ are the control functions and p the time-invariant model parameters for a certain time horizon $\tau = [0, t_f]$. An example of invariant parameter is the constant radiation emissivity ϵ. The goal of the optimal control problem (OCP) is to find the control trajectory $u(\cdot)$ in the time horizon $\tau = [t_0, t_f]$ that minimizes a certain objective function or cost function Φ.

In this case, the objective function contains only a Lagrange-type term L defined as the accumulated value:

$$\Phi(x(\cdot), u(\cdot), p) = \int_0^{t_f} L(x(t), u(t), p)dt, \qquad t\epsilon\tau. \tag{16}$$

Where L consists of two penalty terms weighted by the constant factors w_1 and w_2:

$$L(x(t), u(t), p) = w_1 \cdot c_T(T) + w_2 \cdot c_P(Power), \qquad t\epsilon\tau. \tag{17}$$

The first penalty term is $c_T(T)$ with $T = T_{out_{BAT}}$, a polynomial which defines the costs associated to the loss of performance and ageing of the HV battery at temperatures outside the optimal range. The second penalty term is $c_P(Power)$ with $Power = \frac{P_{LV}}{\eta} + P_{Chiller}$, a linear function that penalizes the electrical power of the LT2 actuators. The weighting factors w_1 and w_2 are used to calibrate the multiple goals achievement, as it will be discussed in the Section IX.

In Fig. 3 the combination of the two penalty terms with the weighting factors $w_1 = 100$ and $w_2 = 2$ is shown from different views. In the bottom plot on the right of Fig. 3, it can be seen that $\approx 28°$C is the optimal temperature for the battery. Colder are less punished than hotter temperatures (slope left to 28°C is smaller than the slope on the right), emphasizing that the aging mechanism is stronger at this range. In the top right plot of Fig. 3 the influence of the power term for a constant temperature is shown. This is the linear function described before. The HV battery temperature has an exponential influence on the costs while the electrical power of the actuators in the LT2 cooling circuit has a linear one.

Additionally to find the minimum of the goal function using the set of ODEs to calculate future states (15), the OCP solution can fulfill some constraints of different types. Taking all this into account, an OCP of the controlled plant can be formulated as:

$$\begin{aligned}
&\min \int_0^{t_f} w_1 \cdot c_T(T_{out_{BAT}}(t)) + w_2 \cdot c_P(\frac{P_{LV}}{\eta} + P_{Chiller})dt \\
&\text{subject to} \\
&\qquad \frac{d(x)}{dt} = f(x(t), u(t), p), t\epsilon\tau, \\
&\qquad 0 \leq c(x(t), u(t), p), t\epsilon\tau, \\
&\qquad 0 = x(0) - x_0.
\end{aligned} \tag{18}$$

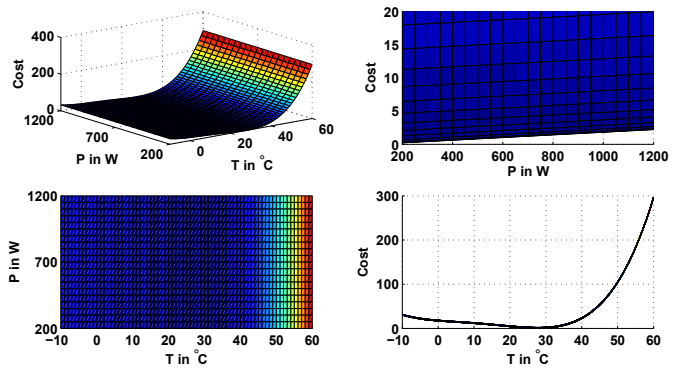

Fig. 3. Different views of the cost function used in the OCP.

where differential states and controls are:

$$x = \begin{pmatrix} T_{in_{PE-PUMP}} \\ T_{in_{BAT-PUMP}} \\ T_{out_{JUNCTION}} \\ T_{out_{CHILLER}} \\ T_{out_{CHARGER}} \\ T_{out_{PE}} \\ E_{BAT} \\ T_{out_{BAT}} \\ T_{out_{COOLER}} \\ v \\ M \\ n \\ T_{ambient} \end{pmatrix} \qquad u = \begin{pmatrix} Valve_{CHILLER} \\ Valve_{CIRCUIT} \\ Pwm_{FAN} \\ Valve_{COOLER} \\ Pwm_{BAT} \\ Pwm_{PE} \end{pmatrix}$$

It must be noted that the differential states v, M, n and $T_{ambient}$ are just inputs from the vehicle, that are kept constant ($\frac{dx}{dt} = 0$) inside the optimization horizon. This will be discussed later, in Section VI. Additionally, the path constraints, $c(x(t), u(t), p)$, used to fix the maximum and minimum acceptable values for the states and controls can be seen in Eq.(19).

$$\begin{aligned} -10^{\circ}C \leq T \leq 60^{\circ}C \\ 1kWh \leq E_{BAT} \leq 8kWh \\ -10km/h \leq v \leq 200km/h \\ -500Nm \leq M \leq 500Nm \\ -10000rpms \leq n \leq 10000rpms \\ 0 \leq Valve_{CHILLER} \leq 1 \\ 0 \leq Valve_{CIRCUIT} \leq 1 \\ 10\% \leq Pwm_{FAN} \leq 90\% \\ 0 \leq Valve_{COOLER} \leq 1 \\ 0\% \leq Pwm_{BAT} \leq 100\% \\ 30\% \leq Pwm_{PE} \leq 100\% \end{aligned} \tag{19}$$

where it must be highlighted that T stands for every temperature state and that the possible values for the valves are 0 (chiller inactive, cooler not bypassed and Two-circuit-mode) and 1 (chiller active, cooler bypassed and One-circuit-mode). Pumps and fan are inactive for the minimum PWM value of 0% and 10% respectively and rotate with full power at 90% and 100%. To avoid unexpected temperature peaks in the PE module, a minimal coolant flow is assured with the PWM constraint of 30%.

Finally, the last constraint in (18) serves to initialize the states:

$$\begin{aligned} T(0) = 20^{\circ}C \quad E_{BAT}(0) = 6.9kWh \quad v(0) = 0km/h \\ M(0) = 0Nm \qquad\qquad n(0) = 0rpms \end{aligned} \tag{20}$$

Once the constrained OCP for the dynamic process is formulated (goal function, equations and constraints), the next step is to obtain the corresponding numerical solution. Notice that the time investment of modeling a system and defining the control problem constrains and goals, is rewarded with the ease of reusability. While for a classical control method changes in the real plant imply the need of a new tuning and analysis of the implemented code, with the NMPC approach it is conceptually easy and fast to modify the Dymola model or the goals, constrains formulated for MUSCODII.

V. Direct Multiple Shooting

For solving an OCP, several methods are available in the literature [31]. The chosen algorithm in this research is the Direct Multiple Shooting Method [32], a numerical method implemented in the robust optimization package MUSCODII. The aim of this method is to transform the infinite optimal control problem of Eq. (18) into a finite dimensional nonlinear programming (NLP) problem. This is done by discretization of the control functions and path constraints and by the parameterization of the state trajectories with the help of a multiple shooting grid:

$$0 = \tau_0 < \tau_1 < \cdots < \tau_N = \tau_f \tag{21}$$

Inside a grid interval, the controls $u(t)$ are approximated by piecewise constant functions:

$$u(t) := q_i \qquad for \qquad \tau \epsilon [\tau_i, \tau_{i+1}), \qquad i = 0, 1...N-1 \tag{22}$$

The state parameterization is done by introducing multiple shooting state variables s_i, that are used as initial values for an embedded initial value problem (IVP) solver that computes the state trajectories independently on N shooting intervals:

$$\frac{d(x_i)(t)}{dt} = f(x_i, q_i, p), \qquad \tau \epsilon [\tau_i, \tau_{i+1}) \tag{23}$$

$$x_i(\tau_i) = s_i \tag{24}$$

Since the N trajectories resulting from the solution of the IVP will not match in the shooting points, to assure continuity between intervals, the following matching conditions have to be satisfied:

$$s_{i+1} = x_i(\tau_{i+1}; \tau_i, s_i, q_i, p) \tag{25}$$

thus requiring that each differential node value s_{i+1} should equal to the final value of the preceding trajectory x_{i+1}. The result of this discretization and parameterization is the highly structured NLP problem of Eq. (26), where the path constraints were discretized for readability and the point constraints grid was chosen to coincide with the shooting grid. The searched unknowns vector ξ consist of the constant control and the initial node value of every interval $\xi := (s_0, s_1 ... s_N, q_0, q_1 ... q_N)$.

$$\begin{aligned} \min_{\xi} \quad & \sum_{i=0}^{N} l_i(\tau_i, s_i, q_i, p) \\ \text{s.t.} \quad & s_{i+1} = x_i(\tau_{i+1}; \tau_i, s_i, q_i, p), \qquad 0 \le i \le N \\ & 0 \le c(\tau_i, s_i, q_i, p), \qquad 0 \le i \le N \\ & 0 = s_0 - x_0. \end{aligned} \tag{26}$$

Eq. (26) is solved by MUSCODII using a tailored sequential quadratic programming (SQP) method that exploits the particular arising structures, using block-wise highrank updates of the Hessian approximation and condensing techniques, to reduce the size of the SQP only to the dimensions of the initial values s_0 and controls $u_0, u_1 ... u_{N-1}$, [23], [32].

VI. Model Predictive Control

The open loop OCP formulation and numerical solution explained in the previous sections would be sufficient to find the controls for the plant to fulfill constraints and minimize the objective function, if no model-plant mismatches and no system disturbances existed. Since this is not the case in the real world, the loop has to be closed as it can be seen in Fig. 4 [33].

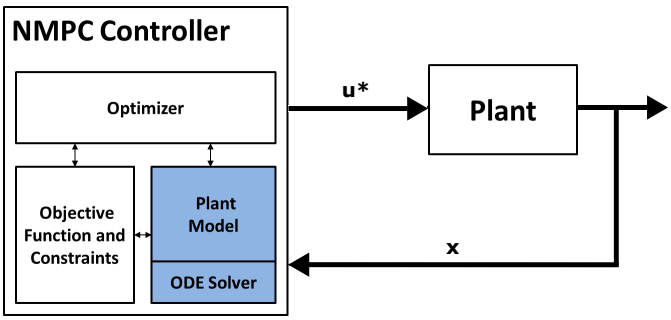

Fig. 4. NMPC control loop scheme.

At each sampling time, the NMPC controller receives the actual state x of the system from the sensors and solves a new OCP to find the best possible control action u^* for that state.

To achieve real time operation and respond quickly to possible disturbances, MUSCODII uses effective strategies presented in [34].

The main idea of these strategies is to exploit the fact that subsequent OCPs differ only in the real-world process state x_0 to reorder the classical SQP scheme advantageously. This new reordered scheme, called real iteration scheme (RTI), consists of the following phases:

- **Preparation phase:** During some process duration δ all steps that do not require knowledge of x_0 are performed. This includes the solution of the IVP, the computation of the Hessian and Jacobians and the linearization of the constrains. The steps of this phase, represent the major computational burden.
- **Feedback response phase:** As soon as a new measurement x_0 is available, the SQP step is computed with the precalculated data in the Preparation Phase to give a fast feedback control to the plant. These control values are maintained during δ, the time needed for the preparation of the next OCP.

Since the feedback phase itself is typically orders of magnitude shorter than the preparation phase the algorithm can be interpreted as the successive generation of immediate feedback laws that take state and control inequality constraints on the complete horizon into account. These calculations are done with computable upper bounds on the loss of optimality [34].

It must be taken into account that the presented NMPC approach, as shown in Section IV, assumes that the inputs v, M, n and $T_{ambient}$ remain constant inside the optimization horizon. While this assumption is generally acceptable for $T_{ambient}$ within a driving cycle, the goodness of the model prediction and thus of the optimization, could be further improved if future information of the mechanical variables v, M, n were available in the vehicle.

Although the prediction of the driving cycle, v profile, with the help of traffic, GPS information has gained attention in recent years [35], at present its implementation has not spread yet. Nevertheless, as soon as a v prediction for the next kilometers is available, the presented model in this paper can be easily extended, to include a mechanical submodel of the traction behavior to calculate the future M and n profiles.

Fig. 5. Test vehicle instrumentation: Coolant flow meters and thermocouples in the motor compartment (left) and air thermocouples on the roof (top right) and in front of the cooler (bottom right).

VII. Real Vehicle Instrumentation

The PHEV prototype used in this research is a Volkswagen Golf GTE, a parallel hybrid electric vehicle with a 1.4 liters 110kW TSI ICE and a 75kW EM. The HV battery with 8.8 kWh provides an electric autonomy of 50 km with a maximum speed in electric mode of 130 km/h.During this study, the vehicle was equipped with extra sensors placed in the LT2 circuit to read all relevant information. In total, 17 K- thermocouples with accuracy of $\pm 1°C$ were used to measure 15 coolant temperatures, the air temperature in front of the cooler and the air temperature on the roof of the vehicle. In addition, three turbine flow meters with a linearity of 0.1% were used to measure the coolant volume flow rate. They were placed in three different points of the cooling circuit to log the flow rates shown in green in Fig. 1. The outputs of these 20 sensors were put together in a single CAN bus by means of several measurement modules. Fig. 5 shows the described instrumentation for this project. Additionally, other available variables in the powertrain- and in the hybrid CAN buses of the vehicle were logged to facilitate the validation by means of a rapid prototyping (RP) module and the INCA environment, both products of ETAS®.

VIII. Validation

To validate the model, different driving cycles were driven. It is important to remark that the LT2 model developed during this research is only valid for the pure electric driving mode, which is the operating mode in daily PHEV use. This condition restricts the total range of a trip to 50km and forces that the trip start point is always the charge station. In Fig. 6, the six different driving cycles chosen to validate the model can be observed.

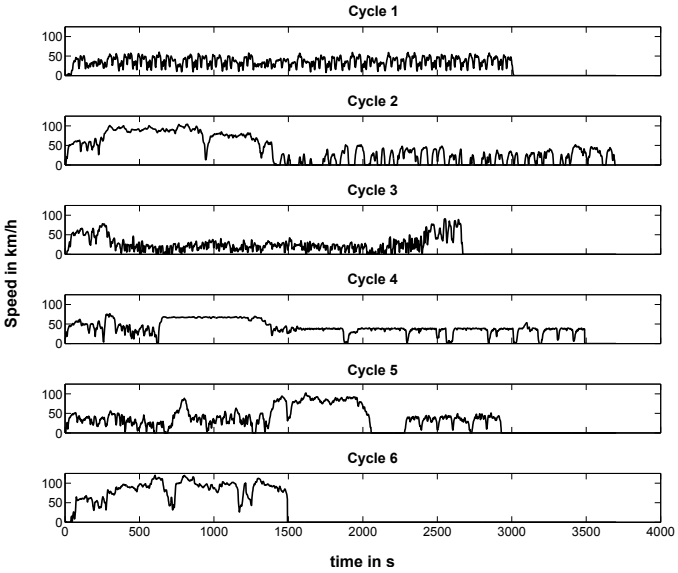

Fig. 6. Driving cycles set chosen for model validation.

Table II summarizes the main features of these trips, where the second column (Type/Road) is a classification in similar term as in [36]. The idea of the driving cycles set of Table II is to grasp a range of possible trips for a driver living in Martorell, a city located at 32km from Barcelona and 10km from the Montserrat mountain. For each cycle in Table II the controls and inputs of the LT2 model were logged.

After driving, this information could be used to simulate the model and compare the measurement/simulation temperature trajectory for the main components of the circuit: battery and power electronics. This error can be defined as:

$$\varepsilon_X = T_{X_{Model}} - T_{X_{Real}}, \qquad X \epsilon \{BAT, PE\} \tag{27}$$

The mean (μ) and standard deviation (σ) for this error can be seen in the last 4 columns of Table II. The battery average error and standard deviation never exceed $1°C$, while the power electronics presents an average error always below $2°C$ with a deviation below $3°C$. As stated before, the goal of the model in a predictive control is to grasp the behavior being, at the same time, fast enough for computation. From this point of view, the obtained results are quite satisfactory.

In the rest of this paper, the focus will be mainly on Cycle 4 due to its considerable slope (about 7%). High slopes represent a heavy mechanical load to the powertrain and in an electric powered vehicle this is a synonym with high currents and indirectly a heavy thermal load in the electrical components.

Fig. 7 shows the goodness of the model for the chosen

TABLE II
VALIDATION RESULTS FOR DIFFERENT CYCLES.

Name	Type/Road	ϕ_{speed}(km/h)	ϕ_T(° C)	$\mu_{\varepsilon_{PE}}$(° C)	$\sigma_{\varepsilon_{PE}}$(° C)	$\mu_{\varepsilon_{BAT}}$(° C)	$\sigma_{\varepsilon_{BAT}}$(° C)
Cycle 1	Urban, free-flowing	35,5	16,7	1,0	0,8	-0,2	0,6
Cycle 2	Motorway + urban unsteady*	39,4	15,0	0,8	-2,4	-0,9	0,5
Cycle 3	Urban, unsteady	26,8	24,1	1,2	0,0	-0,5	0,5
Cycle 4	Rural road + slope	41,8	22,5	1,1	-1,1	-0,8	0,5
Cycle 5	Motorway + secondary rural roads	41,1	20,4	1,2	-2,8	-0,4	0,3
Cycle 6	Main road, steady speed	80,9	22,8	1,8	0,0	0,0	0,7

*cycle with more frequent acceleration and deceleration

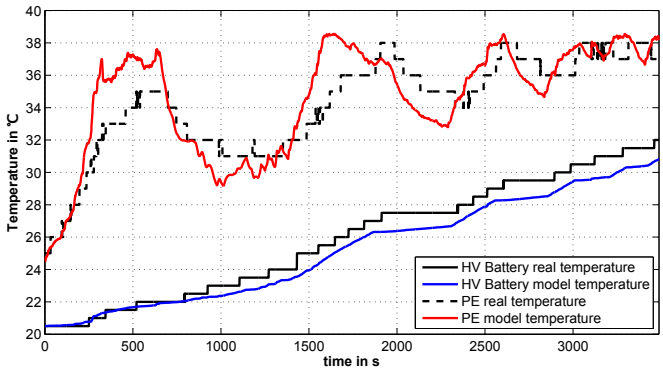

Fig. 7. The model captures the LT2 circuit behavior.

driving cycle, since it captures the transient dynamics of the components temperatures reliably.

IX. RESULTS

A necessary step before implementing the control in the real vehicle is to validate the NMPC in a simulation environment. With this aim, Cycle 2 and Cycle 4 were performed on the road to measure the vehicle speed, electric machine torque and rotational speed, ambient temperature and the LT2 controls. With this data, the two following simulations were performed:

- **Standard simulation:** where the TM controls and the other variables logged in the vehicle are used in the Dymola model of Section III as control signals and inputs stored in look-up tables, respectively, to simulate the cycle.

- **NMPC simulation:** where the software in the loop (SIL) in Fig. 8 is performed. Here, the look-up tables containing the mechanical inputs and ambient temperature acquired on the road together with the Dymola model of Section III, built the controlled plant that is connected to MUSCODII. Controller and plant communicate by means of the co-simulation environment TISC Suite from TLK Thermo GmbH [37].

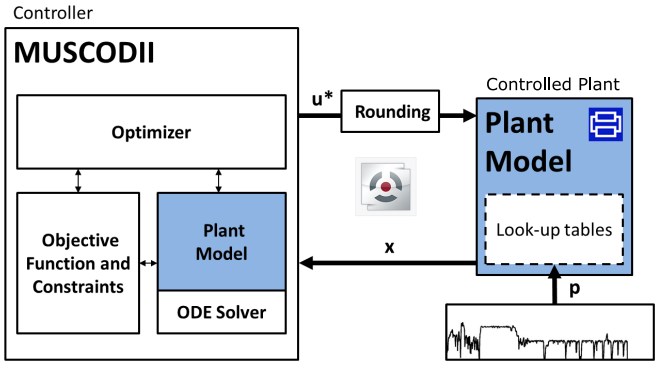

Fig. 8. Software in the loop.

It must be added that the co-simulation tool TISC Suite performs the data transfer and the synchronization between Dymola and MUSCODII with a synchronization rate of 2.5 seconds, which is a valid number for the inertia of the studied thermal system. Notice that since in this simulation evaluation model and controlled plant match exactly, disturbance effects are neglected.
On the other hand, it is important to say that the ”standard” control is based on a finite-state machine with 4 possible states: heating, maintaining temperature, mild cooling and maximal cooling. Depending on the current BAT temperature and some sensors describing the availability of the heat exchangers to dissipate the heat, it fixes the current state where the 6 control variables are given certain constant values.

Additionally, as shown in the ”Rounding” box in Fig. 8, although more suitable strategies to deal with integer control variables exist, [38], [39], here the simple approach of solving the original OCP and rounding the values of the binary variables was taken given the already high system complexity. Hence, the valves

controls sent by MUSCOD that are equal or greater than 0.5 are taken as 1, and 0 otherwise.

A. NMPC calibration process

Prior to analyzing the NMPC control strategy, it is interesting to highlight the process of calibrating the weighting factors, w_1 and w_2, in the objective function. With this aim, Cycle 2 due to its transient behavior was chosen to study the effect of these factors in the TM results.

In the top plot in Fig. 9, the black solid line shows the vehicle speed which was performed in a highway road followed by a traffic jam in the entrance of Barcelona. The red solid line in the middle plot in Fig. 9 shows the BAT temperature profile obtained in a simulation where the standard controls measured in the vehicle were used as inputs. The colored areas in the plot represent the goodness of the temperature region for the BAT, being the dark green area the optimal range. The other two solid lines stand for the temperature response obtained with the NMPC control strategy using a power consumption weighting factor of $w_2 = 0$, black line, and $w_2 = 2$, blue line. The temperature weighting factor is taken constant and equal to 100.

As it can be seen in the middle plot, the NMPC control strategy achieves, with the two different calibrations, a better temperature regulation than the standard control strategy, since the temperatures obtained are closer to the optimal range. Furthermore, it must be noticed that the NMPC with no power consumption costs, $w_2 = 0$, black line, achieves the best temperature performance.

In the bottom plot in Fig. 9, the electrical consumption of the actuators can be seen where the NMPC with no consumption costs presents the largest value at the end of the cycle. The reason for this behavior is that using a zero weighting factor for the consumption, the NMPC control strategy does not penalize this term and concentrates only on improving the temperature regulation, goal that achieves successfully, as mentioned before.

Comparing the standard control results, red line, with the NMPC with non-zero consumption weighting factor, it can be said that, besides the commented improvement in the temperature regulation, a reduction of 7.6% in the electrical consumption can be observed in the bottom plot in Fig. 9. Therefore, it can be assured that the $w_1 = 100$ and $w_2 = 2$ NMPC configuration leads to a better TM improving significantly the two control goals. Furthermore, it must be highlighted that the tuning process of an NMPC controller is quite intuitive and straightforward, since varying the weighting factor associated to an objective, leads to a cosnequent change in the objectives trade-off.

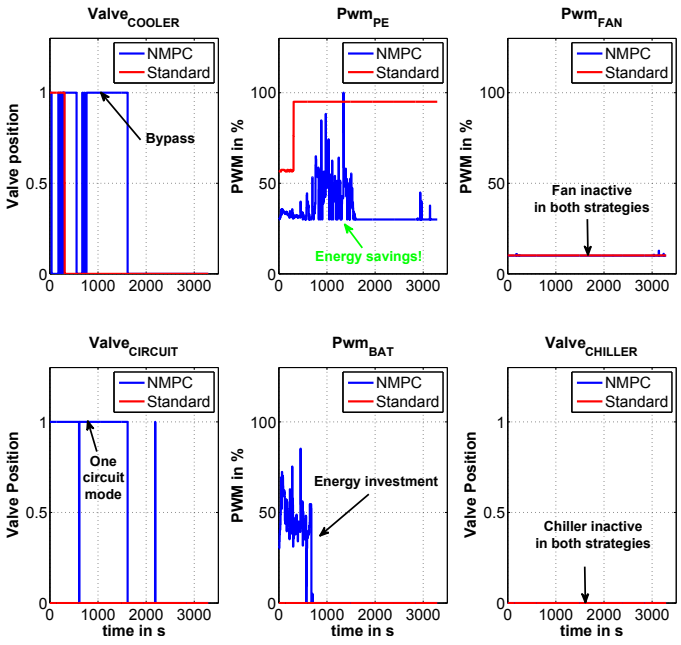

Fig. 11. NMPC controls (in blue) vs Standard controls (in red).

B. Standard vs NMPC results analysis

Figure 10 shows Cycle 4, which consists of a rural road followed by a considerable slope (dotted line in the top plot of Fig. 10) in which the vehicle is driven uphill and downhill at nearly constant speeds (solid line in the top plot of Fig. 10). The initial state of the BAT is fully charged and the data acquisition system is stopped as soon as the electric mode is no more available and the vehicle turns on the ICE at time 3488s.

The bottom plot in Fig. 10 summarizes the advantages of using NMPC, in blue, instead of the standard control strategy, in red. From the temperatures point of view, it can be clearly seen, that drawing from a suboptimal temperature in the BAT (20°C), NMPC achieves a faster heating to the optimal range, green area in Fig. 10.This objective is achieved consuming 15.6 Wh or 5.56% less electrical energy in the actuators as it can be seen in the black line of Fig. 10. Thus it can be said that NMPC succeeded in the multiple objective achievement for the studied TM. How this was achieved, can be understood if we analyze the controls in both strategies shown in Fig. 11.

Given that Cycle 4 is a moderate-intense cooling scenario (temperatures around 20 - 30 °C) but not extreme, both methods agree in the decision of avoiding the usage of the most consuming actuators: the chiller and the fan

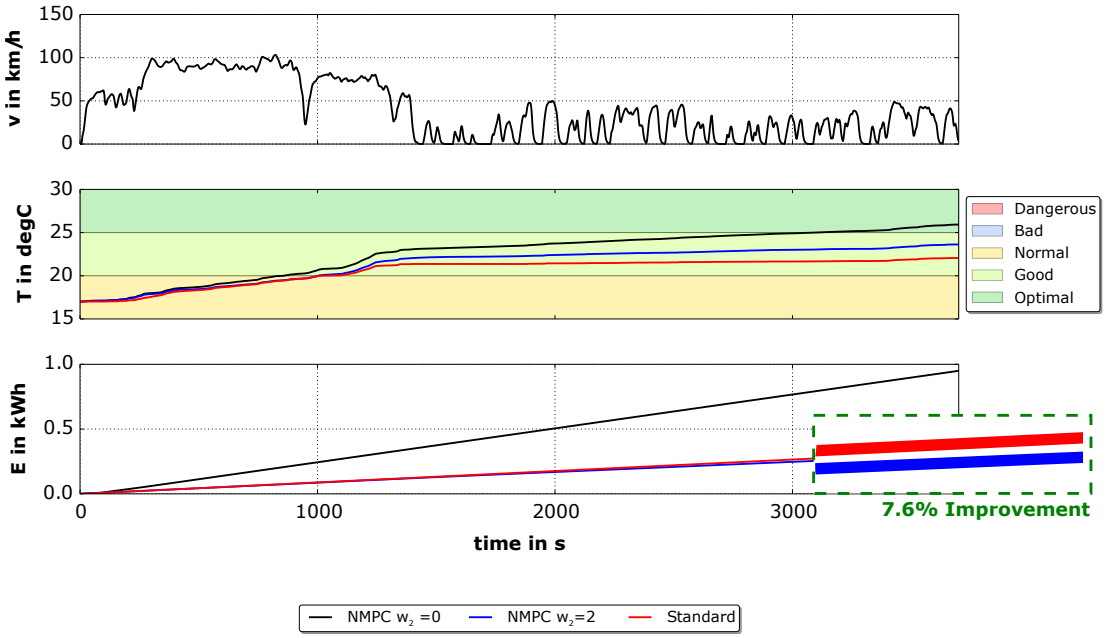

Fig. 9. NMPC tuning process for Cycle 2.

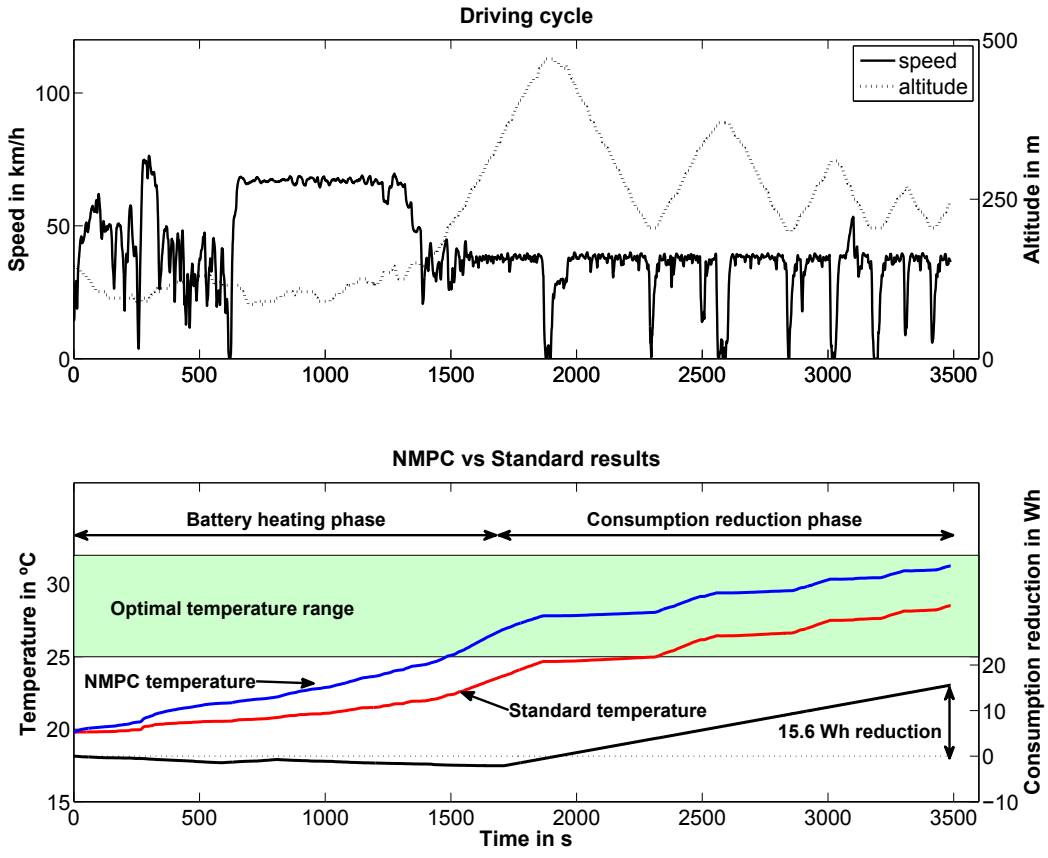

Fig. 10. NMPC vs Standard results for Cycle 4.

(top and bottom plots on the right in Fig. 11) in order to decrease electrical consumption. However, the main differences of both strategies can be seen in the four plots on the left of Fig. 11 where while the standard control strategy presents two clear different operating points (First 300s: Two-circuits-mode, cooler bypassed,

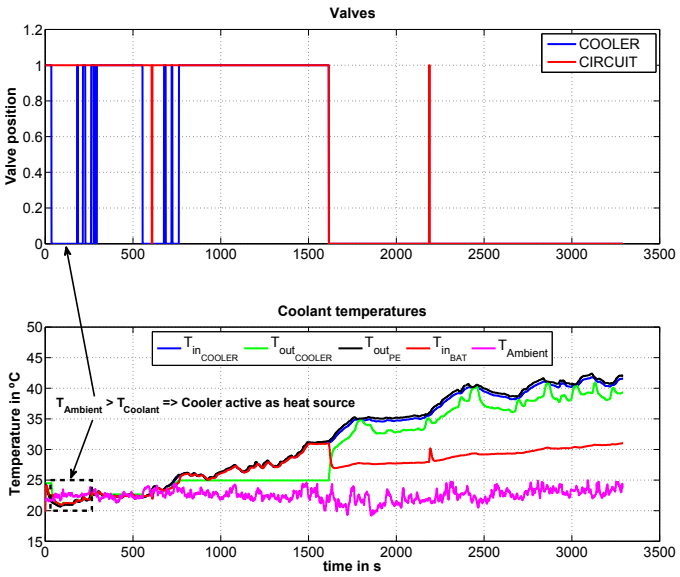

Fig. 12. NMPC control of the valves (top) and coolant temperature in different points.

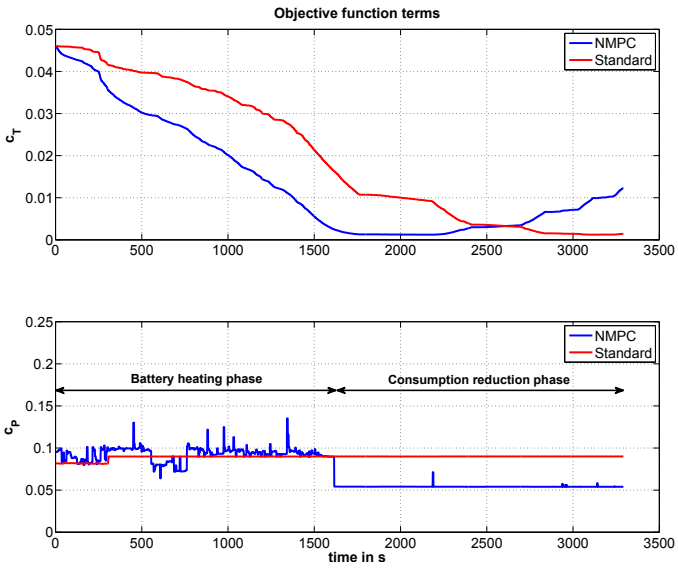

Fig. 13. NMPC (blue) vs Standard (red) penalty terms.

$Pwm_{PE} = 57\%$ and $Pwm_{BAT} = 0\%$; 300s-end: Two-circuits-mode, cooler active, $Pwm_{PE} = 95\%$ and $Pwm_{BAT} = 0\%$), the NMPC shows a dynamic behavior using different circuit configurations to minimize the goals contained in the objective function.

The advantage of such dynamic behavior is a more efficient use of the available resources. This can be clearly seen in Fig. 12, where during the short period between 30 and 260s (black dotted rectangle in the bottom) in which the ambient temperature is higher than the coolant, the valves are set to the one circuit mode/ cooler active configuration ($Valve_{CIRCUIT} = 1$, $Valve_{COOLER} = 0$ in red and blue in the top plot, respectively) to enable the heat transfer between the hot air and the BAT. This way, the components are warmed up. Once the coolant is warmer than the ambient air, the cooler is bypassed ($Valve_{COOLER} = 1$) and the battery remains coupled to the big circuit to be heated solely by the PE, which has a lower thermal mass. As soon as the optimum temperature of the battery is reached (around t = 1700s), the circuits are separated ($Valve_{CIRCUIT} = 0$). From this moment, the goal is to minimize consumption as it can be seen in the Fig. 13, where the cost related to the electrical consumption c_P decreases from second 1700.

This multi-objective character of NMPC can be seen with more details in Table III, where the numerical results in objective function and total consumption terms for the standard, the NMPC and the NMPC without rounding control strategies are shown. The fourth column shows that NMPC achieves an improvement in the overall costs associated to the TM around 31% which split in the different goals, implies a reduction in the electrical consumption of 5% together with a more suitable control of the BAT temperature.

Furthermore, Table III indicates that the prize to pay for the rounding of the control valves is not so significant in terms of the goal function: An improvement of 30.98% is achieved without rounding, while the improvement with rounding is 30.08%. Additionally, it has a positive effect in the power consumption term (5.23% improvement compared to standard rounding against 5.56% without rounding). Even if the rounding approach is dangerous from the optimality criteria scope, the experience in this case shows a suitable behavior doing this simplification. What can be assured is that the decision of replacing the solenoid valves of the LT2 cooling circuit with proportional valves would lead to better results in general, since in the NMPC without rounding the optimizer can choose between possible values $\epsilon[0, 1]$ and as it could be seen here, the optimal solution often uses values that are between these limits.

Finally, besides the successful results it must be added that with the configuration used, horizon of 200s, 2 shooting points and the weighting factors w_1 and w_2 100 and 2 for the studied cycle, it was observed that in average MUSCOD-II needs only 1.5 seconds for calculating the controls, which are transmitted every 2.5 seconds. These NMPC results suggest that the system could be suitable for real-time performance in the real vehicle.

X. Conclusions

A nonlinear model predictive control (NMPC) for the thermal management (TM) of Plug-in Hybrid

TABLE III
OPTIMIZATION RESULTS.

	Standard	NMPC not round		NMPC round	
	Total	Total	Improvement to Standard	Total	Improvement to Standard
ϕ Objective function	2,196	1,516	30,98 %	1,535	30,08 %
Consumption	0,280 kWh	0,266 kWh	5,23 %	0,265 kWh	5,56 %

Electric Vehicles (PHEV) is presented. Compared to a non-predictive standard control based on a finite-state machine, the proposed NMPC application has shown a reduction of 30% in the costs associated to the PHEVs thermal management. Furthermore, it has been shown that a further advantage of the proposed method is its quite simple tuning process.

The proposed NMPC has been tested in a PHEV carrying out six different driving cycles, and its results materialize in healthier temperatures of the HV Battery along the cycle, fast warm up and more time in good temperature range, consuming, at the same time, 5% less electrical energy.Furthermore, the SIL test performed has shown that the proposed application can be used to identify and test potential measures for the cooling circuit, such as the conclusion that replacing the solenoid valves with proportional valves would lead to slightly better results for the treated cooling circuit. With the SIL test it has also been checked that real time implementation with the proposed configuration is possible, making this work a necessary first step for the online NMPC implementation of the analyzed system. Currently, the online coupling of MUSCODII with the real vehicle by means of a rapid prototyping module is being studied together with the use of driving cycle future information.

Another advantage of the proposed application is its reusable structure. The model and the optimization formulation developed permit straight ahead modifications to easily implement NMPC in other cooling circuit architectures.

REFERENCES

[1] A. Heidi, R. Sampsa, O. Juha, T. Anu, and A. Toni, "Process to support strategic decision - making : Transition to electromobility," in *EVS27 International Battery, Hybrid and Fuel Cell Electric Vehicle Symposium*, 2013, pp. 1–8.

[2] S. Al-hallaj, R. Kizilel, A. Lateef, R. Sabbah, and J. R. Selman, "Passive Thermal Management Using Phase Change Material (PCM) for EV and HEV Li- ion Batteries," pp. 1–5.

[3] E. Karden, B. Fricke, T. Miller, and K. Snyder, "Energy storage devices for future hybrid electric vehicles," *Journal of Power Sources*, vol. 168, pp. 2–11, 2007.

[4] J. Axsen, A. Burke, and K. S. Kurani, "Batteries for Plug-in Hybrid Electric Vehicles (PHEVs): Goals and the State of Technology circa 2008," Institute of transportation studies UC Davis, Tech. Rep., 2008.

[5] T. Yuksel and J. Michalek, "Development of a Simulation Model to Analyze the Effect of Thermal Management on Battery Life," Carnegie Mellon University, Tech. Rep., 2012.

[6] R. Mahamud and C. Park, "Reciprocating air flow for Li-ion battery thermal management to improve temperature uniformity," *Journal of Power Sources*, vol. 196, no. 13, pp. 5685–5696, 2011.

[7] S. Al-hallaj and J. R. Selman, "Thermal modeling of secondary lithium batteries for electric vehicle / hybrid electric vehicle applications $," *Journal of Power Sources*, vol. 110, pp. 341–348, 2002.

[8] G.-h. Kim, J. Gonder, J. Lustbader, and A. Pesaran, "Thermal Management of Batteries in Advanced Vehicles Using Phase-Change Materials," *The World Electric Vehicle Journal*, vol. 2, no. 2, pp. 134–147, 2008.

[9] J. Gonder, J. Lustbader, A. Pesaran, and N. Renewable, "Thermal Management of Batteries in Advanced Vehicles Using Phase Change Materials," *The World Electric Vehicle Journal*, vol. 2, no. 2, pp. 134–147.

[10] A. A. Pesaran, "Battery Thermal Management in EVs and HEVs : Issues and Solutions," in *Advanced Automotive Battery Conference*, Las Vegas, Nevada, 2001.

[11] E. Kim, K. G. Shin, and J. Lee, "Real-time battery thermal management for electric vehicles," *2014 ACM/IEEE International Conference on Cyber-Physical Systems (ICCPS)*, pp. 72–83, 2014.

[12] P. Qingfeng, F. Yunzhou, and Z. Xiangbing, "Battery thermal management system design and control strategy study for hybrid electric vehicles," *2014 IEEE Conference and Expo Transportation Electrification Asia-Pacific (ITEC Asia-Pacific)*, pp. 1–4, 2014.

[13] D. Hrovat, S. Di Cairano, H. Tseng, and I. Kolmanovsky, "The development of Model Predictive Control in automotive industry: A survey," *2012 IEEE International Conference on Control Applications*, pp. 295–302, 2012.

[14] M. Huang, H. Nakada, and K. Butts, "Nonlinear Model Predictive Control of a Diesel Engine Air Path : A Comparison of Constraint Handling and Computational Strategies," in *5th IFAC Conference on Nonlinear Model Predictive Control*, no. 2014, Seville, 2015.

[15] J. S. D. S. Laila and A. J. C. P. Fussey, "Nonlinear Model Predictive Control for Cold Start Selective Catalytic Reduction," *IFAC-PapersOnLine*, vol. 48, pp. 471 – 476, 2015.

[16] J. E. Hadef, S. Olaru, P. Rodriguez-ayerbe, G. Colin, and Y. Chamaillard, "Nonlinear Model Predictive Control of the Air Path of a Turbocharged Gasoline Engine Using Laguerre Functions," in *System Theory, Control and Computing (ICSTCC), 17th International Conference*, 2013, pp. 193–200.

[17] N. V. Duijkeren, T. Keviczky, and P. Nilsson, "Real-Time NMPC for Semi-Automated Highway Driving of Long Heavy

Vehicle Combinations," in *5th IFAC Conference on Nonlinear Model Predictive Control*, Seville, 2015.

[18] M. Canale, L. Fagiano, and V. Razza, "Vehicle lateral stability control via approximated NMPC : real time implementation and software in the loop test," *Automatica*, no. 2, pp. 4596–4601, 2009.

[19] S. Di Cairano, D. Yanakiev, A. Bemporad, I. V. Kolmanovsky, and D. Hrovat, "Model predictive idle speed control: Design, analysis, and experimental evaluation," *IEEE Transactions on Control Systems Technology*, vol. 20, no. 1, pp. 84–97, 2012.

[20] M. Josevski and D. Abel, "Flatness-based Model Predictive Control for the Fuel Optimization of Hybrid Electric Vehicles," in *5th IFAC Conference on Nonlinear Model Predictive Control*, Seville, 2015.

[21] H. Esen, T. Tashiro, D. Bernardini, and A. Bemporad, "Cabin Heat Thermal Management in Hybrid Vehicles using Model Predictive Control," in *22nd Meditteranean Conference on Control and Automation (MED)*, Palermo, 2014.

[22] F. Pizzonia, T. Castiglione, and S. Bova, "A Robust Model Predictive Control for efficient thermal management of internal combustion engines," *Applied energy*, vol. 169, pp. 555–566, 2016.

[23] H. G. Bock and K. J. Plitt, "A multiple shooting algorithm for direct solution of optimal control problems," in *Proceedings 9th IFAC World Congress Budapest*, vol. XLII, 1984, pp. 243–247.

[24] H. Jelden, K. Philipp, N. Weiss, and A. Kessler, "The Plug-In Hybrid of the Volkswagen Modular Transverse Matrix," *MTZ*, vol. 75, no. Development Alternative Drives, pp. 18–25, 2014.

[25] L. Del Re, P. Ortner, and D. Alberer, "Chances and challenges in automotive predictive control," in *Lecture Notes in Control and Information Sciences*, L. Del Re, Ed. Springer, 2010, vol. 402, pp. 1–22.

[26] D. AB, "Dymola Users Manual Version 5.3a," Lund, Sweden, 2004.

[27] C. C. Richter, "Proposal of New Object-Oriented Equation-Based Model Libraries for Thermodynamic Systems," PhD Thesis, TU Braunschweig Fakultät für Maschinenbau, 2008.

[28] P. von Böckh and T. Wetzel, "Erzwungene Konvektion," in *Wärmeübertragung Grundlagen und Praxis*. Springer, 2011, ch. 3.

[29] T. J. Barlow, S. Latham, I. S. Mccrae, and P. G. Boulter, "A reference book of driving cycles for use in the measurement of road vehicle emissions," Department for Transport TRL Limited, Tech. Rep., 2009.

[30] M. Gräber, C. Kirches, D. Scharff, and W. Tegethoff, "Using Functional Mock-up Units for Nonlinear Model Predictive Control," in *Proceedings of the 9th International Modelica Conference*, Munich, 2012.

[31] M. Diehl, H. Ferreau, and N. Haverbeke, "Efficient numerical methods for nonlinear MPC and moving horizon estimation," in *Nonlinear Model Predictive Control*, L. Magni, Ed. Springer, 2009, pp. 391–417.

[32] D. B. Leineweber, I. Bauer, H. G. Bock, and J. P. Schlöder, "An efficient multiple shooting based reduced SQP strategy for large-scale dynamic process optimization. Part 1: Theoretical aspects," *Computers and Chemical Engineering*, vol. 27, no. 2, pp. 157–166, 2003.

[33] M. Diehl, R. Findeisen, S. Schwarzkopf, I. Uslu, F. Allgöwer, H. G. Bock, E.-D. Gilles, and J. P. Schlöder, "An Efficient Algorithm for Nonlinear Model Predictive Control of Large-Scale Systems Part I: Description of the Method (Ein effizienter Algorithmus für die nichtlineare prädiktive Regelung großer Systeme Teil I: Methodenbeschreibung)," p. 557, 2002.

[34] M. Diehl, H. G. Bock, J. P. Schlo, R. Findeisen, Z. Nagy, and F. Allgo, "Real-time optimization and nonlinear model predictive control of processes governed by differential-algebraic equations," *Journal of Process Control*, vol. 12, pp. 577–585, 2002.

[35] J. J. Valera, B. Heriz, G. Lux, J. Caus, and B. Bader, "Driving cycle and road grade on-board predictions for the optimal energy management in EV-PHEVs," *EVS27 International Battery, Hybrid and Fuel Cell Electric Vehicle Symposium*, pp. 1–10, 2013.

[36] M. Andr, "Real-world driving cycles for measuring cars pollutant emissions Part A: The ARTEMIS European driving cycles," Institut National de Recherche sur les Transports et leur Securite, Cedex, Tech. Rep., 2004.

[37] R. Kossel, N. Christian, S. Wilhelm, T.-t. Gmbh, T. U. Braunschweig, and I. Thermodynamik, "Effects of Tool Coupling on Transient Simulation of a Mobile Air-Conditioning Cycle Co-simulation," in *Proceeedings 7th Modelica Conference*, Como, 2009, pp. 20–22.

[38] S. Sager, "Numerical methods for mixed-integer optimal control problems," *Praxis*, no. 2005, p. 219, 2006.

[39] M. Gerdts and S. Sager, "Mixed-Integer DAE Optimal Control Problems : Necessary Conditions and Bounds," pp. 189–212.